Disorder phenomena in the incommensurate compound $Bi_{2+x}Sr_{3-x}Fe_2O_{9+\delta}$

O. Pérez, H. Leligny, D. Grebille
Laboratoire CRISMAT (URA CNRS 1318), ISMRA, Boulevard du Maréchal Juin, 14050 Caen CEDEX, France

J. M. Grenêche
Laboratoire de physique de l'état condensé (URA CNRS 807), Université du Maine, 72017 Le Mans CEDEX, France

Ph. Labbé, D. Groult, and B. Raveau
Laboratoire CRISMAT (URA CNRS 1318), ISMRA, Boulevard du Maréchal Juin, 14050 Caen CEDEX, France

(Received 29 April 1996)

The refinement of the modulated structure of $Bi_{2+x}Sr_{3-x}Fe_2O_{9+\delta}$, using the four-dimensional formalism and single-crystal x-ray-diffraction data, has been performed. Different models, already used for the copper compound, have been tested to describe the [BiO] layers. A discussion pointing out the qualities and the failings of each one led us to consider a model assuming a static disorder both on the bismuth and oxygen atom positions. Then, an extra oxygen atom has been located within the [BiO] layers and its occupancy probability has been refined. Because of this model, two disordered regions, governing the behavior of all the atoms in the crystal, have been evidenced. A comparison with the supercell description previously reported shows the interest of the four-dimensional formalism in this case. Finally, a Mössbauer study of $Bi_{2+x}Sr_{3-x}Fe_2O_{9+\delta}$ specifies the trivalent state of iron and confirms the various surroundings in oxygen atoms of the iron atoms. The correlation between the incommensurate character of the structure and the Mössbauer spectroscopy data is discussed. [S0163-1829(97)03502-9]

I. INTRODUCTION

The structural properties of the $Bi_2Sr_2Ca_{n-1}Cu_nO_{2n+4}$ superconducting copper oxides are still not completely understood because of intrinsic difficulties: incommensurate modulation, oxygen stoichiometry, crystal synthesis, and morphology. The related iron compounds have also been synthesized[1–3]. They exhibit the same type of structural features and a better understanding of their structure and of their magnetic properties is helpful for the description of the electronic behavior of both types of compounds. Schematically, the two basic crystal structures can be described, as usual, from an intergrowth between rocksalt- and perovskite-type layers, normal to the $\vec{c}$ direction. The rocksalt-type layers are similar. They are built up of two parallel BiO slices which can occasionally accommodate, because of the displacive modulation, a supplementary oxygen. The perovskite layers of the two oxides are rather different. In the Cu compound, the oxygen-deficient central plane is only occupied by Ca atoms and is bordered on each side by a pyramidal oxygen copper layer. Cu is located near the basal plane of the pyramid, forming four short Cu-O distances of about 1.9 Å and one longer apical Cu-O distance of about 2.4 Å. All the strontium atoms lie near the O plane parallel to $(\vec{a}, \vec{b})$. On the other hand, in the Fe compound (Fig. 1), the central plane is occupied both by Sr(2) atoms and O(4) atoms. The substitution of Fe(III) for Cu(II) implies, indeed, the existence of additional O(4) atoms in such a way that the double pyramidal copper layer is replaced by a double octahedral iron layer. This structure exhibits a modulation characterized by the wave vector $\vec{q^\star} = q_2^\star \vec{b^\star} + \vec{c^\star}$ similar to the copper oxide. Up to now two variants of the $Bi_{2+x}Sr_{3-x}Fe_2O_{9+\delta}$ compound have been observed: either with a rational value of $q_2^\star$ [0.2 (Ref. 4)] or an irrational one [0.212(1) (Ref. 5)]. In the study of the commensurate variant of the iron compound, Lepage *et al.*[4] found the presence of an extra oxygen atom within the BiO layers. Recently, other authors[6–9] also proposed various interpretations concerning the oxygen nonstoichiometry within the BiO layers in the related copper oxides. In all these studies, however, a common anomaly with

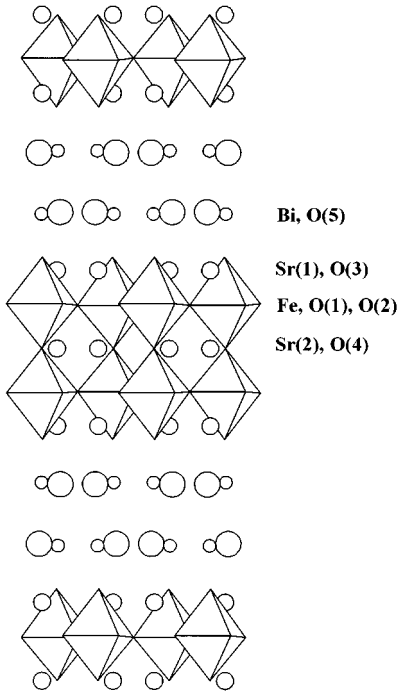

FIG. 1. Average structure of the $Bi_{2+x}Sr_{3-x}Fe_2O_{9+\delta}$ compound.

 © 1997 The American Physical Society

respect to unusually large displacement parameters for some bismuth and strontium atoms can be pointed out.

Moreover, in a recent study of the incommensurate iron compound,[5] we noted some difficulties with a satisfactory explanation of a part of the refinement results for the bismuth atoms. A static disorder and/or a possible lowering of the translation lattice symmetry were postulated. Unfortunately, none of these hypotheses could be tested owing to the small size of the crystals.

More recently, an improvement of the crystal growth has allowed a larger single crystal to be obtained, which in turn makes possible more reliable structural studies. In the present work, atom locations and occupancies in intermediate rocksalt-type layers involving both [BiO] and [SrO] layers are accurately determined. Correlations of the changes in the Fe-O distances, occupation of strontium sites, and oxygen nonstoichiometry with Mössbauer spectroscopy data at 77 and 293 K are also discussed.

II. EXPERIMENTAL DETAILS

Single crystals of the $Bi_{2+x}Sr_{3-x}Fe_2O_{9+\delta}$ phase have been prepared from a mixture of $SrCO_3$, Fe_2O_3 and an excess of Bi_2O_3 with a small amount of PbO as a flux. The powders with the molar ratio Bi:2.43 Sr:1.98 Fe:1 Pb:0.25 were thoroughly mixed and then heated in an alumina crucible first to 850 °C during 2 h, held for 24 h, then heated to 1150 °C during 1 h, held for 2 h, and slowly cooled to 950 °C at a rate of 1 °C /h. The charge was finally cooled to room temperature at a rate of 300 °C /h. Crystals were cleaved along the ab plane. A single monodomain crystal with a size of $0.14\times0.23\times0.005$ mm^3 and a good crystalline quality (sharp diffraction spots, no diffuse streaks) was chosen for the diffraction study. The unit cell parameters are as follows: $a=5.477(1)$ Å, $b=5.464(1)$ Å, and $c=31.685(5)$ Å. Intensities of 1298 unique reflections with $I>3\sigma(I)$, including 602 first and 223 second-order satellites, were measured using Mo $K\alpha$ radiation on Enraf Nonius diffractometer at room temperature using the SAT (Ref. 10) program. Analytical absorption corrections, based on the crystal morphology, were applied using the REMOS (Ref. 11) program.

Mössbauer resonance spectra were recorded at 77 and 293 K with a polycrystalline sample using a conventional constant acceleration spectrometer and a ^{57}Co/Rh source. Least-square refinements were performed assuming a sum of Lorentz functions by means of the computer program MOSFIT (Ref. 12).

III. MODULATED STRUCTURE

A. Characterization of the $\vec{q}^{\star}$ vector

The modulation vector of the present iron oxide compound is very close to the corresponding one of the copper oxide compound. Its $q_2^{\star}$ component was refined by a least-square fit using the Bragg angles of 12 independent first-order satellite reflections and it equals to 0.2070(8).

This value slightly differs from 0.212(1) reported in Ref. 5 for different single crystals and from 0.211(1) for a $Bi_{2+x}Sr_{3-x}Fe_2O_{9+\delta}$ powder. These different values are probably due to small differences in x and in δ or to a small insertion of Pb from the flux in the sample.

B. Symmetry

In our previous study,[5] the reflection conditions seemed to be consistent with a face-centered lattice. The larger size of the present crystal allowed us to detect weak reflections which required a lowering of the translation lattice symmetry from a face centered to a base centered.

Considering the generalized diffraction vector $\vec{s}^{\star}=h\vec{a}^{\star}+k\vec{b}^{\star}+l\vec{c}^{\star}+m\vec{q}^{\star}=H\vec{a}^{\star}+K\vec{b}^{\star}+L\vec{c}^{\star}+mq_2^{\star}\vec{b}^{\star}$, the following conditions were observed: $HKLm$ $K+L+m=2n$, compatible with the four-dimensional Bravais class $mmmA(0,\gamma,1)$; $HK0mm=2n$, compatible with a mirror $(^{m_z}_{s})$; and $0KLm$ $K=2n$, compatible with a mirror $(^{b_x}_{1})$.[13,14] The present setting choice is equivalent to the standard one $mmmA(00\gamma)$ using $\vec{a'}^{\star}=\vec{a}^{\star}$, $\vec{b'}^{\star}=-\vec{c}^{\star}$, $\vec{c'}^{\star}=\vec{b}^{\star}$, and $\vec{q'}^{\star}=\vec{b}^{\star}+\vec{c}^{\star}-\vec{q}^{\star}$. It allows us to describe the modulation of the iron compound with the same modulation vector as in the case of the related copper oxide. Two superspace groups are compatible with the previous conditions: the centrosymmmetric one $Abmm(0,\gamma,1)00s$ and the noncentrosymmetric one $Ac2m(0,\gamma,1)s0s$.

Note that the occurrence of an octahedral metal coordination in the present iron oxide instead of a pyramidal one like in the related copper oxide leads to an A-centering instead of a B-centering one. As a matter of fact, the symmetry group of the copper oxide would constrain the x_3 displacement of the new oxygen atom O(4) to zero while with the present superspace group the mirror $(^{m_z}_{s})$ allows this expected displacement.

C. Structure refinement

A displacive character was taken into account for all the atoms and modelized by atomic displacements $\vec{U}(\overline{x_4})$ expanded in Fourier series of the internal parameter $\overline{x_4}=\vec{q_i}.\langle\vec{r_0}\rangle+\alpha$, where $\langle\vec{r_0}\rangle$ is the average atomic position and α is a phase variable in the [0,1] range, following

$$U_i(\overline{x_4})=\sum_n\ [A_{i,n}\cos(2\pi n\overline{x_4})+B_{i,n}\sin(2\pi n\overline{x_4})].$$

An occupation modulation was also introduced for Bi, Fe, and O(5) atoms and a modulation of substitution of Sr for Bi on Sr(1) and Sr(2) sites was also considered. The occupancy probability is also expanded in a similar manner:

$$P(\overline{x_4})=\langle P\rangle+\sum_n\ [A_n\cos(2\pi n\overline{x_4})+B_n\sin(2\pi n\overline{x_4})].$$

As satellite reflections were measured only up to the second order, only two orders of harmonics were introduced in the preceding relations. As will be discussed in the following section, the Bi and O(5) atoms were displaced from their special position in the mirror plane m_y to a general position. The modulated structure was refined assuming the $Abmm(0,\gamma,1)00s$ SSG, with the F magnitudes and unit weights using the JANA (Ref. 15) program. Final agreement factor is $R_G=0.047$ (0.039, 0.049, and 0.075 for the main

and first- and second-order satellite reflections, respectively). The results of the refinement are given in Table I

The amplitudes of the displacive modulation functions are shown in Figs. 2 and 3 as a function of the phase variable α. As was already generally mentioned, the displacement amplitudes along c increase gradually from the Bi layers to the Sr(2) layers while an opposite effect occurs for the displacements along $\vec{b}$. Another property is illustrated by the variation of the Bi-Bi interatomic extralayer and intralayer distances (Fig. 4), which are opposite in phase in particular around $\alpha \simeq 0.75$; the shorter extralayer distances correspond to the larger intralayer ones, to expanded zones, while the other parts of the crystal can be considered as compressed zones.

IV. DISORDER WITHIN THE BiO LAYERS

In the present study, particular attention has been paid to the [BiO] layers which present common structural features with the related ones in the superconducting Cu oxides. The refinement of the site location and occupancy of oxygen atom within the [BiO] layers is important to clarify the global oxygen stoichoimetry, but is difficult because of the weak scattering capability of oxygen for x rays. Moreover, a reliable solution requires a better understanding and description of the modulation of the heavy Bi atoms, for which thermal motion anomalies have been previously outlined.

A. Modulated split atom model for Bi atoms

In a previous study,[5] the thermal mean-square displacement of Bi atoms along the $\vec{a}$ axis was found to be abnormally high. As a result a disordered model has been proposed with a splitting of the bismuth atoms along $\vec{a}$. In the present study, the lowering of translation symmetry from F to A removes this anomaly. A refinement of Fourier terms for thermal parameters was attempted for Bi atoms. It still resulted in abnormal large β_{22} values in some unit cells of the crystal which are still to be explained.

This anomaly is always present in the iron and the copper compounds.[4,6,9,16,17] The thermal modulation of the bismuth atom involves large Fourier terms which cannot be easily interpreted. Moreover, the strong correlation between thermal agitation and occupation probability can artificially improve the refinement results without any obvious physical meaning, and so disturbs the determination of other structural parameters as modulated displacements or site occupancies. A static disorder of the bismuth atoms was considered in the present model rather than a thermal modulation.

The average position of the bismuth atom was splitted along the $\vec{b}$ axis and the modulated displacement along this direction was allowed to vary. The distance Bi(a)-Bi(b) (Fig. 5) between the two corresponding symmetry-related sites presents a significant maximum (0.4 Å) around $\alpha \simeq 0.75$ in agreement with a static disorder in the expanded zones. Hereafter, the related disordered region will be denoted $D1$. Elsewhere, as the Bi(a)-Bi(b) distance is smaller than 0.1 Å, no definitive conclusion can be given about the splitting of the sites.

The $Ac2m(0,\gamma,1)s0s$ SSG was also tested, with an unique bismuth site, but leads to the same problem concerning the Bi thermal mean-square displacement. So in this case, two independent sites were also necessary. Moreover, using this noncentrosymmetric SSG some problems of least-squares convergence were encountered.

B. Oxygen sites

In the previous studies,[4,6,7] two types of oxygen sites were introduced in the [BiO] layers. The first one corresponds to a usual rocksalt position, the second one to a bridging position. Then, there are two ways to explain the excess of oxygen. Either the rocksalt position is fully occupied and the bridging site is partly occupied in one cell out of five, corresponding to the expanded zones of the layer (model I), or one can imagine a description of the rocksalt position with a ''saw-toothlike function''[6,15]

$$U_i = 2U_0(x_4 - x_4^0)/\Delta.$$

Δ values greater than 1 allow an overlapping of these functions which can describe the simultaneous occupation of two O(5) sites apart from each other and leading to an average occupation of the rocksalt site greater than 1 (model II). In the latter case, the bridging position is not taken into account and the two models differ by the x_1 and x_3 components of the average position of the extra oxygen.

In the present study, the x_2-x_4 section of the four-dimensional Fourier difference map (Fig. 6), calculated after introduction of all atoms including the two bismuth sites but without the oxygen atom, shows a very large displacive modulation along the $\vec{b}$ axis, for this O(5) atom. Moreover, the corresponding string is discontinuous along x_4, which is not the usual behavior for a simple displacive modulation function, and appears as a sequence of oblique strips displaying overlapping regions for $x_4 = 0.75$. These regions coincide with the disordered $D1$ regions. This unusual feature can be explained assuming a static disorder on the O(5) sites as can be evidenced from the x_1-x_2 section map (Fig. 7). As the Fourier maps look very similar to that calculated in the copper compound with model II, this approach was tested in the present case in a model assuming a centrosymmetric or a noncentrosymmetric SSG. Our results for the $Abmm(0,\gamma,1)00s$ SSG are summarized in Table II (model II). In all cases, the linear function does not account for the actual shape of the electronic density and, in particular, in the overlapping disordered regions where the displacement amplitudes became too large. Moreover, in this model, unrealistic Bi-O distances (<1.5 Å) were calculated. The refined value of Δ was not significantly different from 1, and could not explain the excess of oxygen. Therefore, this model seems to be inappropriate in the present case.

Model I was also tested in the case of the copper compound[17] in a modulated subcell description involving both displacive and occupation modulations, using Fourier series terms up to the second order. In order to describe the title compound, a similar model was tested. However, only the rocksalt site could be refined (Table II, model I). This site explains about 80% of the electronic density drawn in Fig. 6. The interatomic Bi-O distances keep reasonable values ($\geqslant 1.9$ Å). However, even if the rocksalt O(5) site globally describes the shape of the electronic density (Fig. 6), it does not still account for the overlapping $D1$ regions (Fig. 7) and

TABLE I. Results of structure refinement.

(a)

Atom		A_0	A_1	B_1	A_2	B_2
Bi(a)	U_1	0.2723(1)	-0.0035(5)	0.0011(4)	0.0 [a]	0.0 [a]
	U_2	0.2626(9)	0.0732(5)	-0.0206(18)	0.0 [a]	-0.0142(4)
	U_3	0.20262(3)	0.0 [a]	-0.00457(5)	-0.00078(7)	0.0007(2)
	P	0.5 [a]	0.0 [a]	0.017(2)	0.031(3)	0.053(7)
Sr(1)	U_1	0.7547(2)	0.0 [b]	0.0 [a]	0.0 [a]	0.0 [b]
	U_2	0.25 [b]	0.0411(5)	0.0 [b]	0.0 [b]	-0.0040(6)
	U_3	0.11738(6)	0.0 [b]	-0.00805(11)	-0.00113(13)	0.0 [b]
	P	0.408(10)	0.0 [b]	-0.034(5)	-0.045(7)	0.0 [b]
Sr(2)	U_1	0.7524(4)	0.0 [a]	0.0 [b]	0.0 [b]	0.0 [a]
	U_2	0.25 [b]	0.0 [a]	0.0 [b]	0.0 [b]	0.0 [b]
	U_3	0.0 [b]	0.0 [b]	-0.01064(15)	0.0 [a]	0.0 [b]
	P	0.25 [a]				
Fe	U_1	0.2509(4)	0.0 [b]	0.0010(9)	0.0 [a]	0.0 [b]
	U_2	0.25 [b]	0.0187(7)	0.0 [b]	0.0 [a]	0.0 [b]
	U_3	0.06029(10)	0.0 [b]	-0.01160(14)	-0.00045(18)	0.0 [b]
	P	0.5 [a]				
O(1)	U_1	0.0 [a]	0.0 [b]	0.0 [a]	0.0 [a]	0.0 [b]
	U_2	0.0 [b]	0.020(6)	0.0 [b]	0.0 [b]	0.0 [a]
	U_3	0.0649(5)	0.0 [b]	-0.0099(7)	0.0 [a]	0.0 [b]
	P	0.5 [a]				
O(2)	U_1	0.5 [a]	0.0 [b]	0.0 [a]	0.0 [a]	0.0 [b]
	U_2	0.0 [b]	0.017(6)	0.0 [b]	0.0 [b]	0.0 [a]
	U_3	0.0674(6)	0.0 [b]	-0.0092(9)	-0.0058(12)	0.0 [b]
	P	0.5 [a]				
O(3)	U_1	0.231(3)	0.0 [b]	0.0 [a]	0.0 [a]	0.0 [b]
	U_2	0.25 [b]	0.084(5)	0.0 [b]	0.0 [b]	-0.036(7)
	U_3	0.1377(4)	0.0 [b]	-0.0030(8)	0.0 [a]	0.0 [b]
	P	0.5 [a]				
O(4)	U_1	0.256(4)	0.0 [a]	0.0 [b]	0.0 [b]	0.0 [a]
	U_2	0.25 [b]	0.0 [a]	0.0 [b]	0.0 [b]	0.0 [a]
	U_3	0.0 [b]	0.0 [b]	-0.0112(9)	0.0 [a]	0.0 [b]
	P	0.25 [a]				
O(5a)	U_1	0.347(3)	0.0 [a]	-0.01(6)	0.0 [a]	0.0 [a]
	U_2	0.876(8)	0.041(11)	-0.074(6)	0.0 [a]	0.0 [a]
	U_3	0.2054(15)	-0.005(3)	-0.0077(11)	0.0 [a]	0.0 [a]
	P	0.50(2)	0.54(5)	0.0 [a]	0.0 [a]	0.0 [a]
O(6)	U_1	0.5 [a]				
	U_2	0.0 [a]				
	U_3	0.178(2)				
	Δ^1, x_4^1	0.13(5)	0.75(5)			

(b)

Atom	B_{eq} or B_{iso}	β_{11}	β_{22}	β_{33}	β_{12}	β_{13}	β_{23}
Bi(a)	0.76	0.0059(1)	0.0058(4)	0.0002(0)	0.0025(7)	0.0 [a]	0.0 [a]
Sr(1)	1.36	0.0049(4)	0.0073(5)	0.0006(0)	0.0 [b]	-0.0004(1)	0.0 [b]
Sr(2)	0.88	0.0042(6)	0.0044(7)	0.0004(0)	0.0 [a]	0.0 [a]	0.0 [b]
Fe	0.63	0.0022(6)	0.0038(7)	0.0003(0)	0.0 [b]	0.0 [a]	0.0 [b]
O(1)	0.7(2)						
O(2)	0.8(2)						
O(3)	1.4(3)						
O(4)	0.9(3)						
O(5a)	1.0(3)						
O(6)	3(1)						

[a]Were fixed during the refinement because they were insignificant.

[b]Are constrained by symmetry.

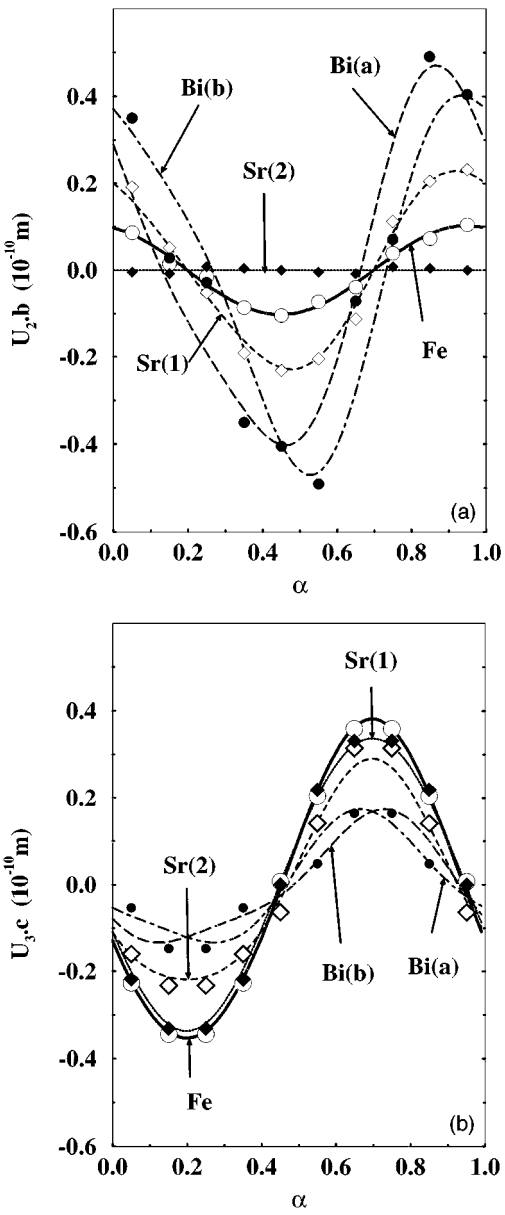

FIG. 2. Modulated cation displacements vs the internal parameter α: (a) along the $\vec{b}$ axis and (b) along $\vec{c}$ axis. Bi(a) and Bi(b) are the two Bi sites related by the $(x,1/2-y,z)$ symmetry operation. Solid circles, open circles, solid diamonds, and open diamonds correspond, respectively, to the atomic displacements of Bi, Fe, Sr(1), and Sr(2) atoms in the supercell description (Ref. 1).

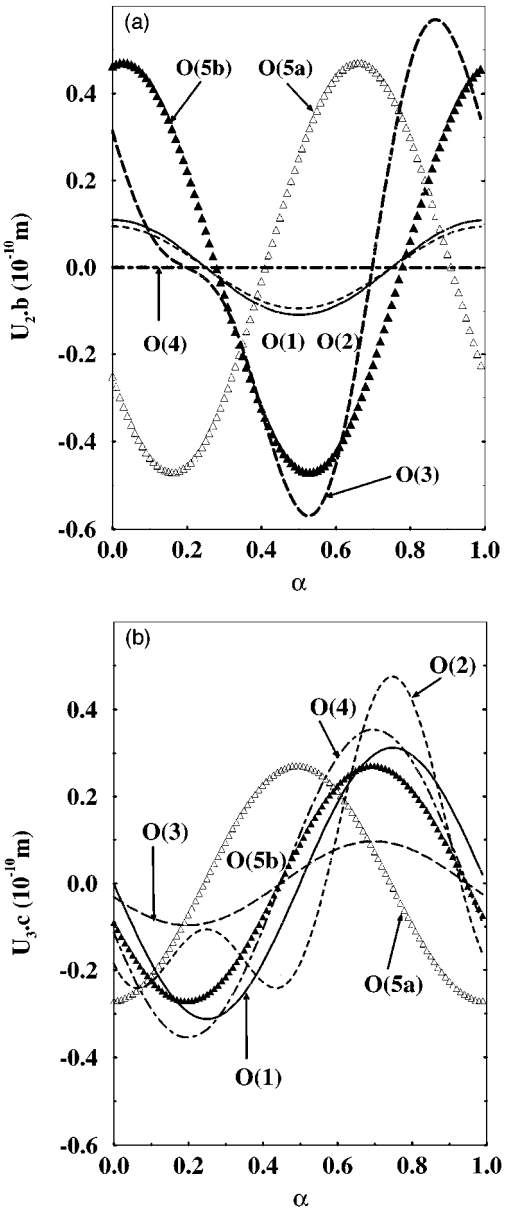

FIG. 3. Modulated oxygen displacements versus the internal parameter α: (a) along the $\vec{b}$ axis and (b) along the $\vec{c}$ axis. O(5a) and O(5b) are the two O(5) sites related by the $(x,3/2-y,z)$ symmetry operation.

this residue cannot be related to the extra bridging oxygen which is located at different x_1 and x_3 coordinates. Moreover, around $x_4 \simeq 0.25$ (modulo 1), the x_1-x_2 section map (Fig. 8) still reveals a splitting of the O(5) site which is not explained by this model. This effect, although smaller than in the $D1$ regions, is significant.

In fact, two types of disordered regions would be involved in the crystal for the O(5) oxygen atoms: the first one denoted $D1$, corresponding to the larger splitting and to the expanded zone, and the second one $D2$, corresponding to a smaller splitting around $x_4=0.25$. In order to describe these split sites in the $D1$ and $D2$ regions with equal occupancy probability, the O(5) atom was replaced by two symmetry-related sites in a general position and then first-order displacive and occupation modulations were introduced. The refinement results are illustrated in Fig. 6 (displacement modulation) and Fig. 9 (occupation modulation). $D1$ and $D2$ regions are now properly described with a half probability of each site when, for $x_4=0.0$ or 0.5, only one site is occupied. The global occupancy of the two preceding sites does not explain the presence of any extra oxygen in the [BiO] layers. In a recent study,[18] a section of the four-dimensional Fourier map containing oxygen atoms in the [BiO] layers in the copper-related compound shows very large similarities with the corresponding present one (Fig. 6). Even if it was not interpreted in terms of double-oxygen site, two maxima are clearly visible and can be explained by the present model.

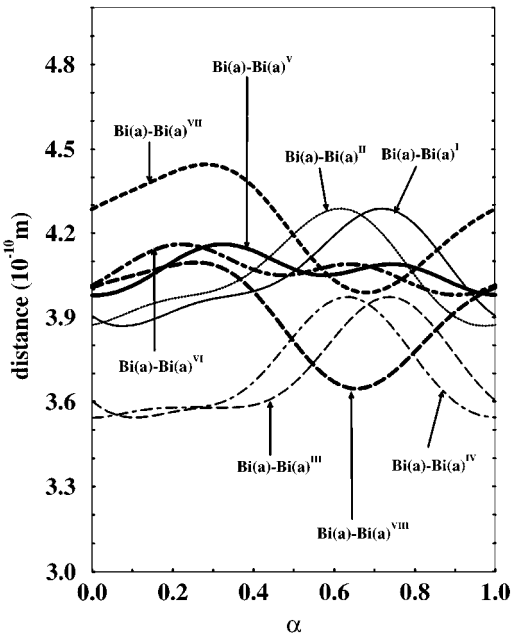

FIG. 4. Interatomic Bi(a)-Bi(a) distances vs the internal parameter α. Bold lines correspond to extralayer distances and thin lines to intralayer distances. (I) $-x,-1/2+y,z$, (II) $-x,1/2+y,z$, (III) $1-x,-1/2+y,z$, (IV) $1-x,1/2+y,z$, (V) $x,-1/2+y,1/2-z$, (VI) $x,1/2+y,1/2-z$, (VII) $-x,y,1/2-z$, and (VIII) $1-x,y,1/2-z$.

Nevertheless, on a x_1-x_2 section of the Fourier difference map, for x_4 corresponding to the $D2$ regions (Fig. 10), a rather diffuse peak appears, with a maximum of $3e^-$ Å^{-3}, at the position of the bridging oxygen described by Lepage *et al.*[4] and in the expanded regions of the BiO layers.

An O(6) oxygen atom was then introduced in the refinement, characterized by a ''crenel function'' for the occupation modulation and without displacive modulation function. The value of the crenel function alternates and is either 0 or 1 on a sequence of intervals. The nonzero interval is centered at $x_4=x_4^1$ and its length is Δ^1 [see Table I(a)].

The O(6) atom shows a large thermal parameter, which is probably the consequence of both the disorder phenomenon and the difficulty of describing a small electronic density using x-ray-diffraction data.

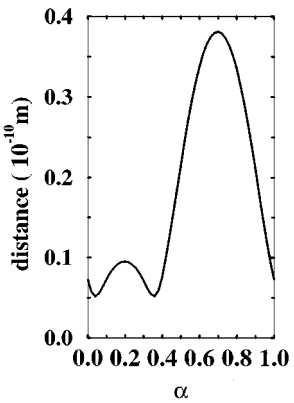

FIG. 5. Interatomic Bi(a)-Bi(b) distances vs the internal parameter α.

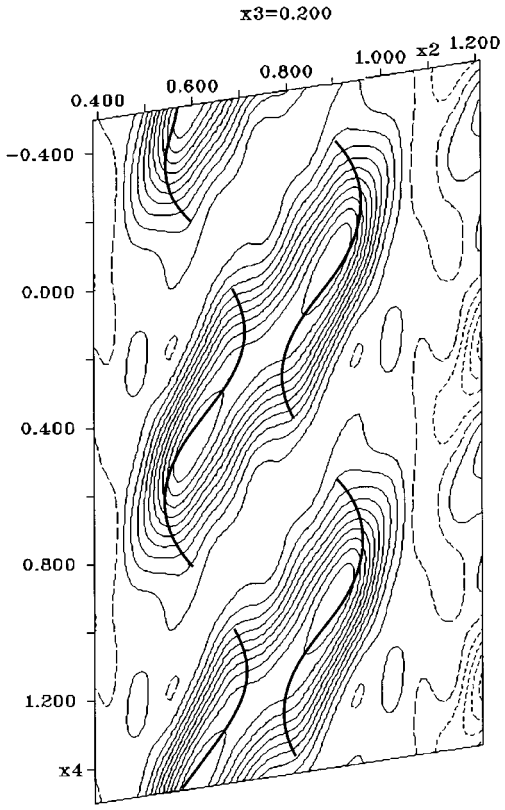

FIG. 6. The section x_2-x_4 ($x_1=0.35$, $x_3=0.205$) of the four-dimensional difference Fourier map. Contours are drawn at intervals of $1e^-$ Å^{-3}. Solid lines, long dashed lines, and short dashed lines represent positive, zero, and negative electron density, respectively. The strings representing the two disordered modulated O(5) sites are drawn as bold lines.

C. Bismuth environment

The variation of the interatomic Bi-O(3), Bi-O(5), and Bi-O(6) distances are drawn in Fig. 11(a). The Bi-O(3) distance is almost constant (around 2.0 Å).

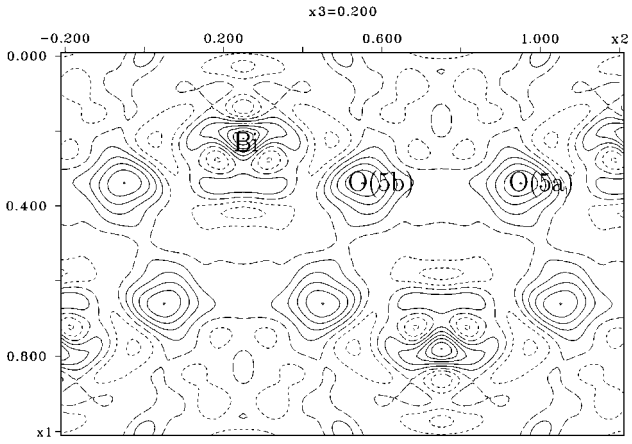

FIG. 7. The section x_1-x_2 ($x_3=0.205$, $x_4=0.75$) of the four-dimensional difference Fourier map showing up the disorder of the O(5) atoms in the $D1$ region. Contours are drawn at intervals of 1 e^- Å^{-3}. Solid lines, long dashed lines, and short dashed lines represent positive, zero, and negative electron density, respectively.

TABLE II. Preliminary models for the O atoms within the [BiO] layers $Abmm$ $(0,\gamma,1)00s$. For model II, $x_4^0=0.255(11)$ and $\Delta=1.0$.[b]

		Model I					Model II	
Atom		A_0	A_1	B_1	A_2	B_2	$\langle U\rangle$	U_0
O(5)	U_1	0.654(3)	0.0[a]	0.0[b]	0.0[b]	0.0[a]	0.346(3)	0.0[b]
	U_2	0.25[a]	0.177(7)	0.0[a]	0.0[a]	-0.032(11)	0.75[a]	-0.299(8)
	U_3	0.202(1)	0.0[a]	0.0[b]	0.0027(12)	0.0[a]	0.201(1)	0.0052(13)
	P	0.78(5)	0.0[a]	0.51(12)	0.25(17)	0.0[a]	1	

[a]Are constrained by symmetry.

[b]Were fixed during the refinement because they were insignificant.

Only the Bi-O(5) distances corresponding to an occupancy of the O(5) sites larger than 0.3 are represented.

The two intralayers Bi-O(5) distances parallel to $\vec{a}$ are also almost constant ($\simeq$3.4 Å and $\simeq$2.2 Å).

The intralayer distances, parallel to the $\vec{b}$ direction of the modulation, vary strongly. They are longer in the $D1$ zones than in the $D2$ zones. Outside the $D1$ zones, one of these distances always keeps a value between 1.8 and 2.4 Å. The Bi-O(6) distances only appear in the $D1$ regions with values between 1.9 and 2.3 Å. As a result, the Bi coordination is always characterized by three short Bi-O bonds ($<$2.3 Å), one around 2.8 Å and two larger ones around 3.4 Å. From the environment of the bismuth ion [Fig. 11(b)] the chemical stereoactivity of this cation in the [BiO] layer is clearly evidenced. One indeed observes a BiO_3 pyramid characterized by three Bi-O short distances with O-Bi-O angles ranging from 87° to 104°. Consequently the $6s^2$ lone pair of bismuth can be oriented in the opposite direction towards the center of the triangle formed by the three other oxygens leading for Bi(III) to a tetrahedral coordination represented by the polyhedron BiO_3L.

D. A possible interpretation

The existence of the $D1$ regions confirms the possible insertion of an extra O(6) atom. As was already mentioned,[9] this insertion is expected to result in the antiparallel displacement of the O(5) atom of these disordered regions, on each side. However, the same effect is also expected for the Bi atom and results for both O atom and Bi atom in two average positions, which have been evidenced in the present study. But now, in the medium zone $D2$ between two adjacent $D1$ regions, the occupation of these new disordered average positions would be too constraining for the Bi environment. A secondary displacement can then be considered to accomodate the cation environment in the $D2$ regions and results in the modulated displacements around the average positions, which counterbalance in these regions the splitting of the average positions. So in the $D2$ regions the two disordered positions are very close to each other. One can in fact consider that in these regions, there are only one Bi site and two equiprobable O(5) sites rather closed to each other. Between the $D1$ and $D2$ regions, O(5) occupies alternately one and the other of the two disordered positions, and the resulting scheme is similar to the periodic alternation of bands, orthogonal to the modulation direction, with antiparallel atomic displacements, already proposed by Levin *et al.*[9] However, in our model, the amplitude of the displacive modulation is reduced and becomes similar to that of the Bi atoms.

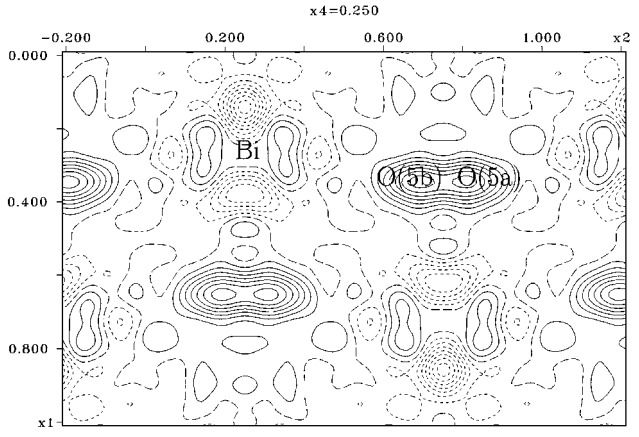

FIG. 8. The section x_1-x_2 ($x_3=0.205$, $x_4=0.25$) of the four-dimensional difference Fourier map showing up the disorder of the O(5) atoms in the $D2$ region. Contours are drawn at intervals of 1 $\overline{e}$ Å^{-3}. Solid lines, long dashed lines, and short dashed lines represent positive, zero, and negative electron density, respectively.

V. STRONTIUM AND IRON ENVIRONMENT

Both the similarity of the modulation functions of the Bi, O(5), Sr(1), and O(3) atoms and the relatively large values of the thermal parameters of Sr(1) and O(3) atoms show that the

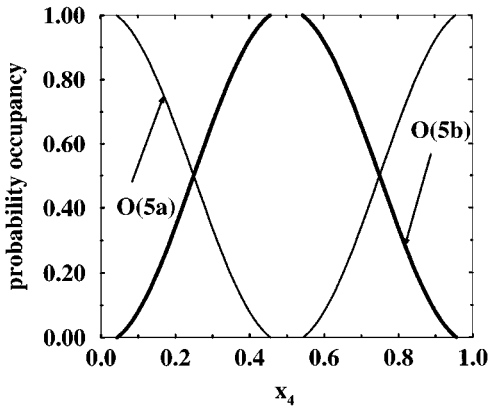

FIG. 9. Occupation probability of the two disordered O(5) sites vs x_4. Solid line, O(5a); dashed line, O(5b).

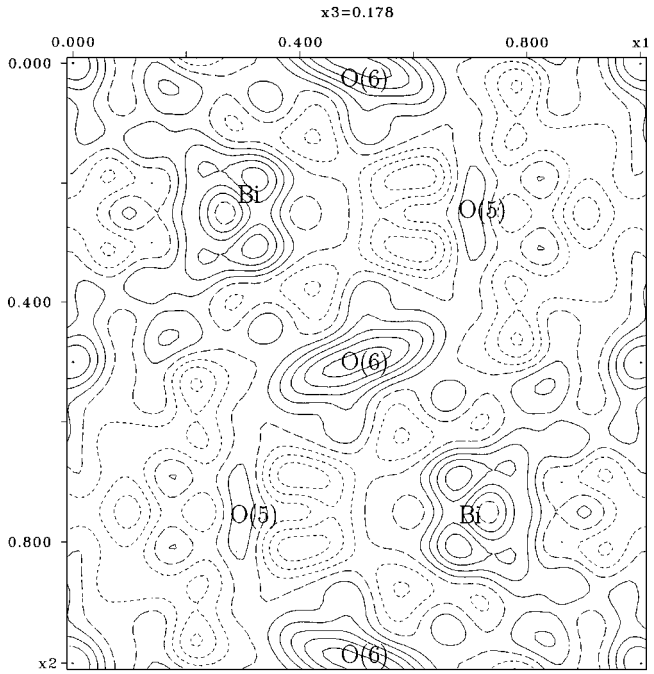

FIG. 10. The section x_1-x_2 (x_3=0.178, x_4=0.25) of the four-dimensional difference Fourier map showing up the extra oxygen O(6). Contours are drawn at intervals of $0.5e\ \text{Å}^{-3}$. Solid lines, long dashed lines, and short dashed lines represent positive, zero, and negative electron density, respectively.

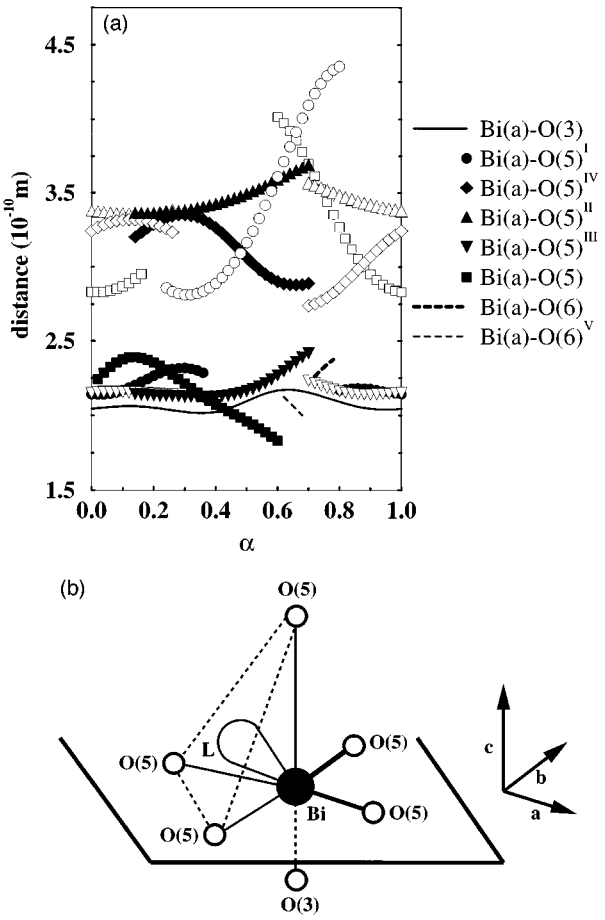

FIG. 11. (a) Interatomic Bi(a)-O distances vs the internal parameter α. The distances Bi(a)-O(5) have been plotted only for an occupation probability $P(\text{O}(5))>0.3$. The distances Bi(a)-O(5a) and Bi(a)-O(5b) are represented, respectively, by open symbols and solid symbols. (I) $x,y-1,z$, (II) $-x,y-1/2,z$, (III) $1-x,y-1/2,z$, (IV) $x,y-1/2,1/2-z$, and V:$1-x,1/2+y,z$. (b) Schematic drawing of the tetrahedral Bi environment.

[Sr(1)O] layers are very influenced by the [BiO] layers and probably characterized by a residual disorder.

The Sr(1) atom is linked to oxygen atoms O(1), O(2), O(3), O(5), and O(6) belonging to the [FeO_2], [Sr(1)O], and [BiO] layers. The Sr(1)-O(3) distances (Fig. 12) present a very large variation. As a result, the Sr(1) site can have an eightfold or a ninefold coordination throughout the crystal. The $D1$ region is still clearly evidenced. The additionnal O(6) atoms are linked to the Sr(1) atom. The distances exhibit reasonable values in the $D1$ regions.

The substitution modulation of Sr for Bi on Sr(1) site is highly significant. The probability of occupancy of the Sr(1) site by bismuth atoms is found to be minimal inside the disordered $D1$ and $D2$ regions (Fig. 13) where the oxygen environment is the less regular.

The variations of the equatorial Fe-O(1) and Fe-O(2) distances and of the apical Fe-O(4) distance are very small, so that the iron atoms are always regularly linked to O(1), O(2), and O(4) atoms. On the opposite the apical Fe-O(3) distance varies strongly between 2.7 Å in the $D2$ regions to 2.15 Å in the $D1$ zones (Fig. 14). As a result, in the $D1$regions, iron displays a less distorted octahedral coordination while in the other zones it displays rather a fivefold pyramidal coordination.

The variation of the Sr(2)-O distances versus α does not cause significant variation of the coordination of the Sr(2) site. It exhibits a regular and constant twelvefold coordination throughout the crystal.

VI. COMPARISON WITH THE PREVIOUS SUPERCELL STUDY

Starting from the atomic positions refined by Lepage *et al.* [4] within the supercell description, it is possible to calculate both the phases and displacements of the different atoms. This work allows us to set up a comparison with our results. Figures 2(a) and 2(b) show the good agreement between the two descriptions concerning the cation positions.

In the particular case of the bismuth atoms, the two curves corresponding to the two disordered sites allow us to account for the dispersion of the representative points of the Bi positions in the supercell approach. Therefore, the hypothesis of a bismuth disorder appears to be a good interpretation of the bismuth behavior and is in agreement with the supercell description.

Moreover, in our study, the two Bi disordered sites have an occupancy of 50%. In fact, taking into account the average position of each site, the two Bi curves are always very close to each other, except in the $D1$ regions, and thus, outside the $D1$ regions, one can assign them to only one Bi site equivalent to the site of the supercell approach. Our study is thereby similar to the supercell approach. In contrast, in the $D1$ zones, the two Bi sites are equally occupied. Lepage *et al.*[4] describe these regions with only one bismuth site. This result can explain the large values of the thermal motion

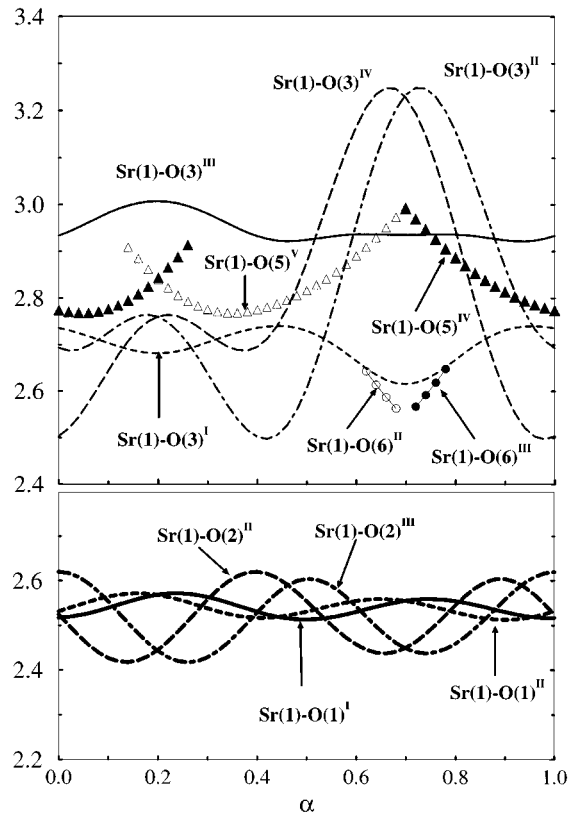

FIG. 12. Interatomic Sr(1)-O distances versus the internal parameter α. The distances Sr(1)-O(5) have been plotted only for an occupation probability $P(\mathrm{O}(5))>0.3$. The distances Sr(1)-O(5) related to a same pair of disordered O(5) are represented with the same symbolism (solid or open). (I) $1+x,y,z$, (II) $1-x,1/2+y,z$, (III) x,y,z, (IV) $1-x,-1/2+y,z$ and (V) $1-x,1-y,z$.

(B_{eq}=2.7 or 2.2 Å^2) observed by these authors for the bismuth atoms in these zones. Such a comparison was not possible for the oxygen atoms, characterized by a large and irregular dispersion in the supercell description. Properly, because of the great number of refinement parameters required for this last description, Lepage *et al.*[4] could not refine all *B* factors for oxygen atoms that were fixed to 1. This can explain the corresponding poor reliability of the oxygen

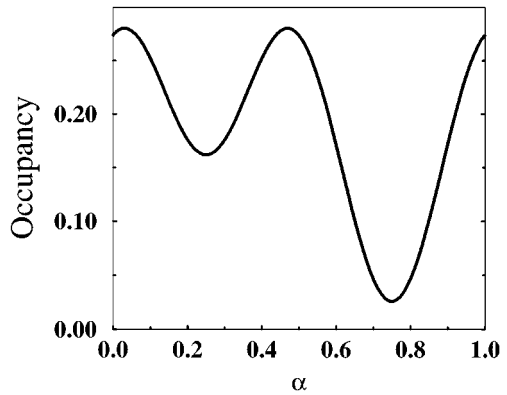

FIG. 13. Occupation probability of the Sr(1) site by bismuth atom vs the internal parameter α.

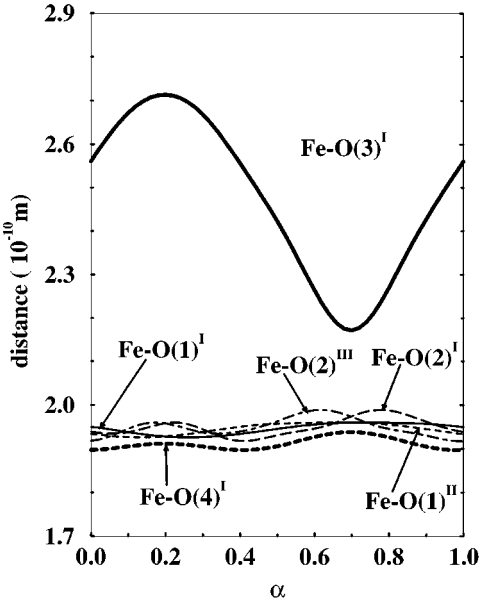

FIG. 14. Interatomic Fe-O distances vs the internal parameter α. (I) x,y,z, (II) $-x,1/2+y,z$, and (III) $1-x,1/2+y,z$.

location in the supercell study. The four-dimensional symmetry considerations have allowed a smaller number of refinement parameters, a better description of the oxygen atoms including disorder and thermal motion, and lead to a more satisfactory residual (0.047 against 0.106). The present description is expected to be more realistic and reliable.

VII. MÖSSBAUER SPECTROSCOPY

The Mössbauer spectra recorded at 77 and 293 K are shown in Fig. 15. At 77 K, the fitting of the spectrum requires at least three Zeeman components, each one with rather broad lines. The values of the isomer shift (IS) and

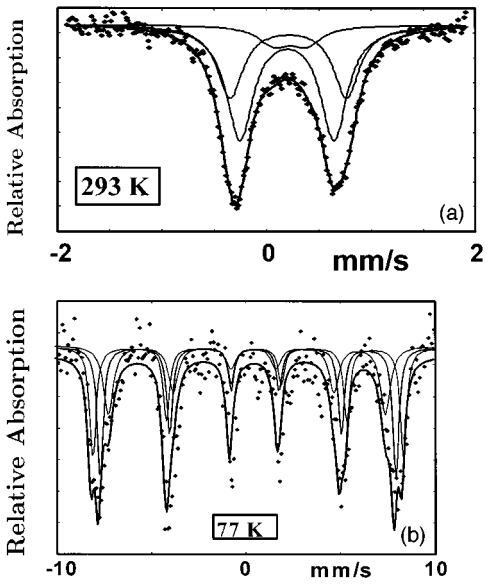

FIG. 15. ^{57}Fe Mössbauer spectra of $Bi_{2.38}Sr_{2.62}Fe_2O_{9.2}$ at 293 K (a) and 77 K (b).

TABLE III. Hyperfine Fe-Mössbauer parameters for $Bi_{2+x}Sr_{3-x}Fe_2O_{9+\delta}$. IS, isomer shift relative to αFe; Γ, half-height width of the doublet; QS, quadrupole splitting; 2ε, quadrupole shift; HF, hyperfine field.

Temperature 77 K					
Site	Type	IS($\pm$0.02) (mm s^{-1})	2ε($\pm$0.02) (mm s^{-1})	HF($\pm$0.02) (T)	Intensity($\pm$5) (%)
A'	Fe^{III}	0.48	-0.46	51	33
B'	Fe^{III}	0.44	-0.40	48	41
C'	Fe^{III}	0.49	-0.38	45	26
Temperature 300 K					
Site	Type	IS($\pm$0.02) (mm s^{-1})	QS($\pm$0.02) (mm s^{-1})	Γ($\pm$0.02) (mm s^{-1})	Intensity($\pm$5) (%)
A	Fe^{III}	0.34	0.30	0.33	10
B	Fe^{III}	0.30	0.89	0.31	58
C	Fe^{III}	0.33	1.10	0.30	32

hyperfine field (HF), listed in Table III, are consistent with ferric ions in a high-spin state. At 293 K, the quadrupolar spectrum consists of two broad and asymmetrical lines. It can be fitted assuming at least the superimposition of three doublets with narrow Lorentzian quadrupole lines; this agrees with the procedure used at 77 K. Values of the isomer shift, quadrupole splitting (QS), and relative intensities of the three components denoted A, B, and C are listed in Table III. The rather small value of the quadrupole splitting of A site (QS = 0.30 mm s^{-1}) is characteristic of a local oxygen environment of the Fe atoms less distorted than those of B and C sites. The appearance of Fe atoms with different local oxygen environments can be explained on the basis of the structural investigation which implies indeed in the $\vec{b}$ direction a complex variation of the apical Fe-O(3) bond length as shown in Fig. 14. Such a variation implies that throughout the crystal, the geometry of the polyhedron varies from an almost regular octahedron in the neighborhood of the $D1$ region to a tetragonal pyramid in the neighborhood of $D2$ regions. As a result, if one assumes that for a Fe-O distance larger than 2.6 Å iron cannot be considered as linked to the apical oxygen O(3), the percentage of Fe(III) in a fivefold coordination can be estimated close to 30% which corresponds to the relative intensity found for the Mössbauer site C (QS=1.10 mm s^{-1}). In the same way, the percentage of Fe(III) in a sixfold coordination with an apical distance close to 2.2 Å can be evaluated to about 10%, in agreement with the relative intensity of the doublet A (QS=0.30 mm s^{-1}). The remaining Fe(III) species can then be distributed in distorted-oxygen octahedra with a mean Fe-O(3) distance close to 2.4 Å in accordance with the Mössbauer site C (QS=0.89 mm s^{-1}). Because of the presence of broad and asymmetrical lines, the quadrupolar spectrum can be reproduced by using a discrete distribution of quadrupole splitting, linearly correlated to that of isomer shift. Each quadrupolar component has fixed natural linewidth during the fitting procedure. At 77 K, only a discrete distribution of hyperfine fields was also considered to reproduce the magnetic spectrum. Such a fitting procedure permits to take into account the broadening of the lines, which generally originates from an amorphous behavior. Further analysis of the resulting distribution of quadrupolar splitting provides information relative to the amorphous state:[19] It concerns the ratio $q=\langle QS^2\rangle/\langle QS\rangle^2$. In the present case, the value of q is equal to 1: This result suggests the presence of a perfect structural order, in spite of the broadening of Mössbauer lines. Also, it is consistent with the incommensurate character of the modulation which leads to a great number of different local iron environments, according to the Fe-O distances, as reported in Fig. 14. Let us mention that the value of $q=1$ established in the magnetically ordered state (77 K) confirms the previous conclusions. Although the linear correlation, introduced between QS and IS in our refinement, has no physical meaning, one can again distinguish three zones according to QS and IS values: The main one corresponds to QS$\simeq$1 mm s^{-1} while the two other ones correspond to QS$\leqslant$0.8 mm s^{-1} and QS$\geqslant$1.1 mm s^{-1} respectively (Fig. 16). In fact, the distribution of the QS values seems to be the best interpretation of the Mössbauer spectra considering the variation of the apical Fe-O(3) distances in Fig. 14 which supposes that the octahedral oxygen environment of iron is more or less distorted depending upon the perturbations due to the modulation wave.

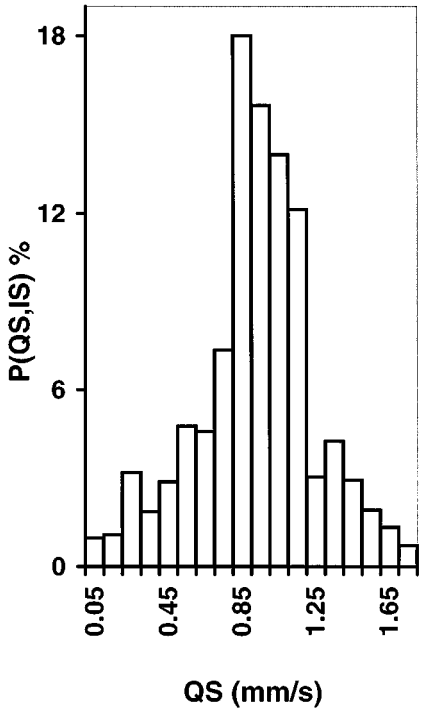

FIG. 16. Evaluated probability distribution of QS at 300 K.

Both the structural investigation of the site occupancies and the Mössbauer study of the iron valence state lead to the chemical formula $Bi_{2.38}Sr_{2.62}Fe_2O_{9.2}$ which corresponds to iron only in the trivalent state Fe(III).

On the other hand, for the $Bi_{2.18}Sr_{1.82}Ca_{0.91}Fe_2O_{9.2}$ ferrite which has been recently studied by Mössbauer spectroscopy,[20] the presence of iron in a mixed valence state involving both trivalent Fe(III) and tetravalent Fe(IV) species has been considered to explain the Mössbauer data at 293 K. Such a result should be ascribed to the lower Bi content which led us to suggest that a possible correlation

should exist between the Bi occupancy of the Sr(1) site and the Fe valence state.

VIII. CONCLUSION

Using a better description of the symmetry of the modulated structure involving less structural parameters and taking into account the actual incommensurate character of the modulation, the four-dimensional formalism has allowed us to give a more accurate description of the $Bi_{2+x}Sr_{3-x}Fe_2O_{9+\delta}$ phase than in the previous supercell description. It appears that in addition to the disorder on the bismuth sites already considered by Grebille *et al.*,[17] a static disorder is likely on the oxygen sites, and both disorders are closely related to each other. They could find their origin in the existence of diluted $D1$ regions where extra oxygen atoms, responsible for the oxygen nonstoichiometry, could insert themselves. The resulting environment of Bi is then compatible with three short distances throughout the crystal.

Two interpretations can be given of the incommensurate character of the modulation. Either the structure is actually incommensurate and this imposes different symmetry configurations for the previous disordered $D1$ and $D2$ zones without any local regular symmetry operator position as suggested by Levin *et al.*,[9] or the occurence of the $D1$ zones is hazardous, resulting in an average period of around $4.83b$. Nevertheless, in both cases, a local disorder for Bi and O atoms must be considered.

Despite the large variations in the Fe environment, the Mössbauer study of the present phase evidenced only a trivalent state Fe(III) for the iron atoms while a mixed valence state involving both Fe(III) and Fe(IV) species has been suggested for the $Bi_2Sr_2CaFe_2O_{9+\delta}$ oxide.[20] However, in these different compounds, the [BiO] layers present quite similar behaviors, in particular concerning the insertion of an extra oxygen atom in the diluted and disordered regions. The balance of charge is then realized either by an excess of Bi for the Ca-free compound or by a mixed valence iron state for the Ca derivative. Thus, it seems to be interesting to study the structure of $Bi_2Sr_2CaFe_2O_{9+\delta}$ in order to compare the two iron compounds and to check up our hypothesis on the relation between [SrO], [BiO], and [FeO] or [CuO] layers if one includes the copper-based Bi 2212 counterpart.

The particular configuration of the [BiO] layers and especially of the $D1$ regions where extra oxygen atoms are interpolated is only made possible by the nonsymmetric environment of bismuth. In this way, the stereoactivity of the $6s^2$ lone pair of Bi(III) is of great importance for the generation of such a situation. This statement is strongly supported by the fact that the introduction of lead in the iron compounds can imply either a change of the modulation vector or the disappearance of the modulation. It is indeed well known that Pb(II), due to its larger size compared to Bi(III), is significantly less stereoactive. A study of the $Bi_{2-x}Pb_xSr_3Fe_2O_9$ oxides is in progress to understand the effects of both Pb and Bi in the modulation of the $Bi_2Sr_2Ca_{n-1}M_nO_{2n+4}$ compounds.

[1] M. Hervieu, C. Michel, N. Nguyen, R. Retoux, and B. Raveau, Eur. J. Solid State Inorg. Chem. **25**, 375 (1988).

[2] R. Retoux, C. Michel, M. Hervieu, N. Nguyen, and B. Raveau, Solid State Comm. **69**, 599 (1988).

[3] M. Hervieu, D. Pelloquin, C. Michel, M. T. Caldes, and B. Raveau J. Solid State Chem. **118**, 227 (1995).

[4] Y. Lepage, W. R. Mc Kinnon, J. M. Tarascon, and P. Barboux, Phys. Rev. B **40**, 6810 (1989).

[5] O. Pérez, H. Leligny, D. Grebille, Ph. Labbé, D. Groult, and B. Raveau J. Phys. Condens. Matter **7**, 1003 (1995).

[6] V. Petříček, Y. Gao, P. Lee, and P. Coppens, Phys. Rev. B **42**, 387 (1990).

[7] A. Yamamoto, M. Onoda, E. Takayama-Muromachi, and F. Izumi, Phys. Rev. B **42**, 4228 (1990).

[8] A. I. Beskrovnyi, M. Dlouhá, Z. Jirák, and S. Vratislav, Physica C **166**, 79 (1992).

[9] A. A. Levin, Y. I. Smolin, and Y. F. Shepelev, J. Phys. Condens. Matter **6**, 3539 (1994).

[10] B. Doudin (private communication).

[11] A. Yamamoto, computer program REMOS, National Institute for Research in Inorganic, Niichari-gun, Ibaraki, Japan, 1990.

[12] F. Varret and J. Teillet, computer program MOSFIT, Université du Maine, Le Mans, France (unpublished).

[13] *International Tables for Crystallography*, edited by A. J.-C. Wilson (Kluwer Academic, Dordrecht, 1982), Vol. C, pp. 797–844.

[14] P. M. De Wolff, T. Janssen, and A. Janner, Acta Crystallogr. A **37**, 625 (1981).

[15] V. Petříček, crystallographic computing system JANA 94 Institute of Physics, Academy of sciences of the Czech Republik, Prague, 1994.

[16] X. B. Kan and S. C. Moss, Acta Crystallogr. B **48**, 122 (1992).

[17] D. Grebille, H. Leligny, A. Ruyter, Ph. Labbé, and B. Raveau, Acta Crystallogr. B **52**, 628 (1996).

[18] Z. Fu, Y. Li, T. Cheng, Y. Zhang, B. Gu, and H. Fan, Sci. Chin. **38**, 210 (1995).

[19] M. E. Lopez-Herrera, J. M. Grenêche, and F. Varret, Phys. Rev. B **28**, 4944 (1983).

[20] V. Sedykh, I. S. Smirnova, A. V. Dubovitskii, B. Zh. Narymbetov, V. Shekhtman, E. V. Suvorov, V. A. Goncharov, and L. A. Novomlinskii, Appl. Phys. A **60**, 71 (1995).